Journal of Aerosol Science 68 (2014) 25–37

Contents lists available at ScienceDirect

Journal of Aerosol Science

journal homepage: www.elsevier.com/locate/jaerosci

Aerosol optical properties in central Argentina

Luis E. Olcese *, Gustavo G. Palancar, Beatriz M. Toselli *

Departamento de Físico Química/INFIQC/CONICET/CLCM, Facultad de Ciencias Químicas, Universidad Nacional de Córdoba, Ciudad Universitaria, 5000 Córdoba, Argentina

ARTICLE INFO

Article history:
Received 4 September 2013
Received in revised form
7 November 2013
Accepted 8 November 2013
Available online 16 November 2013

Keywords:
Córdoba region
AERONET
Aerosol optical properties
Inter annual variation
Back trajectories

ABSTRACT

This work presents the analysis of the long-term observations of aerosol optical properties in the central region of Argentina. Monitoring of aerosol parameters was carried out at the Cordoba-CETT AERONET site (31° 31′ S, 64° 27′ W, 730 m.a.s.l.) from November 1999 until December 2010. Long-term measurements of aerosol optical depth, Ångström exponent, fine mode fraction and single scattering albedo were analyzed and compiled to describe the climatology of the optical properties of the aerosols of the region. The knowledge of the optical properties of aerosols and their spatial distribution is required to evaluate aerosol effects on the climate system. This information provides an opportunity for understanding how aerosols might influence the regional radiation budget. Results show that aerosol optical depth at 340 nm is characterized by low values from February to April (monthly average of 0.15 ± 0.05), very low values from May to June (monthly average of 0.08 ± 0.03) and a sustained increase from July to September (monthly average of 0.20 ± 0.09) reaching a value of 0.26. From this dataset, no long-term trends are observable. Results of the inter-annual variations of the Ångström exponent between 440 and 870 nm reflect an important difference in the year 2004 compared to the other 11 years of the study. A possible explanation of this fact is elaborated with the help of back trajectory analysis. Finally, three episodes are described and analyzed, as they produced important increases of the daily aerosol optical depth value. We explained these episodes with a combination of air mass trajectory analysis, meteorology and the MODIS fire counts product.

1. Introduction

Atmospheric aerosols and pollutants absorb and scatter shortwave solar radiation and these interactions have resultant impacts on atmospheric radiative transfer balance (Solomon et al., 2007). Atmospheric aerosol particles in the boundary layer can also significantly change air quality either directly or by affecting the rate of tropospheric ozone formation (Flynn et al., 2010). Scattering by aerosols increases the actinic flux and the rates of photochemical reactions in the upper parts of the planetary boundary layer, while aerosol absorption reduces the amount of UV radiation available for chemical reactions within and below the aerosol layer. Therefore, without accurate knowledge of aerosol UV absorption, the magnitude and even the sign of the aerosol effect on tropospheric photochemistry will remain highly uncertain (Palancar et al., 2013).

* Correspondence to: Departamento de Físico Química / INFIQC, Facultad de Ciencias Químicas, Universidad Nacional de Córdoba, Pabellón Argentina, Ciudad Universitaria, 5000 Córdoba, Argentina. Tel.: +54 351 4334169; fax: +54 351 4334188.
E-mail addresses: lolcese@fcq.unc.edu.ar (L.E. Olcese), tosellib@fcq.unc.edu.ar, tosellib@yahoo.com.ar (B.M. Toselli).

0021-8502/$ - see front matter © 2013 Elsevier Ltd. All rights reserved.
http://dx.doi.org/10.1016/j.jaerosci.2013.11.003

When aerosols are emitted into the atmosphere from some natural or anthropogenic sources, it is important to know its further behavior. The questions to answer are: how far and how fast particles can be transported? What are the dimensions of the plume during the transport? If we measure the aerosol properties at a given site, how much of these properties are determined by local sources and how much by distant ones? Since many of the involved parameters are highly dependent on weather conditions and on the topography of terrain, all these questions are not easy to answer.

In order to analyze the association between trajectories and air mass composition arriving at a site, a multitude of methods to carry out trajectory classifications has been devised (Fleming et al., 2012) and references therein. Over the last decades, trajectory analysis has been widely used to examine the dynamical processes and the patterns of the air mass transport. In a review of recent aerosol studies in Europe it was found that 11% of all studies used back trajectory methods to cluster aerosol levels according to their origins and transport pathways (Viana et al., 2008).

Optical properties of aerosols transported by an air mass can be obtained either from satellite or surface measurements. Satellite data can provide the required space-time coverage of aerosol optical depth (AOD) but the retrieval of aerosol absorption, in the form of single scattering albedo (SSA), is not reliable compared to the ground-based measurements (Zawadzka et al., 2013). Ground-based measurements of aerosol properties are more accurate than the satellite observations and have a better temporal resolution, but they are limited in the spatial distribution. In the last two decades, a large number of studies dealing with the analysis, retrieval, or estimation of aerosol optical properties from ground measurements have been published (e.g. Dubovik et al., 2000; Srivastava et al., 2012).

In spite of its importance, only a few works dealing with optical properties of aerosols have been published for the central region of Argentina. In one of these studies, Andrada et al. (2008) used their irradiance dataset, the AERONET (AErosol Robotic NETwork) database, and the TUV (Tropospheric Ultraviolet and Visible) model (Madronich, 1987) to analyze the effects of aerosols on surface Ultraviolet B irradiance (UV-B, 280–315 nm) on cloudless days in Córdoba city, Argentina, during the period 1999–2006. More recently Achad et al. (2013) used individual particle analysis and experimental UV-B irradiance measurements together with radiative transfer calculations to retrieve and compare the relative contribution of aerosol types at an urban site of the Córdoba city. Beyond the few works about aerosol optical properties published for Córdoba region, at present and as far as we know, there are no studies relating their optical properties with the pathways of the air masses arriving to this region.

In this work, we first present a comprehensive analysis of the aerosol optical properties measured at the Cordoba-CETT (Centro Espacial Teófilo Tabanera) AERONET site in the period of 1999–2010 and then the correlation of these properties with the pathway of the air masses arriving at the site during a long period of anomalous values. As the instrument measuring in this AERONET station was deployed at another place in 2010, the analyzed period represents the whole and only dataset of ground-based aerosol properties for the central region of Argentina. Back trajectories calculated for this period by using the Hybrid Single-Particle Lagrangian Integrated Trajectory model (HYSPLIT 4) were clustered to show the climatology of the air masses arriving to the region according to both position and frequency. In addition, the analysis of the daily, monthly, annual, and inter annual variation of the aerosol optical properties allowed to detect episodes, which are explained considering the meteorology of the region and the origin and transport of the air masses.

2. Materials and methods

2.1. Site and meteorology

The measurement site is a rural area located 20 km to the West of Córdoba city. A few kilometers to the West of the site, the so-called *Sierras Chicas* range of hills runs in the North-South direction for 490 km, with an average height of 800 m.a.s.l. and a few peaks, no higher than 2000 m.a.s.l.

The aerosol optical parameters were measured with a CIMEL Electronique 318A Sun photometer deployed at Cordoba-CETT AERONET station (31° 31′ S, 64° 27′ W, 730 m.a.s.l.) in 1999. This instrument provides AOD values at seven spectral bands (340, 380, 440, 500, 670, 870, and 1020 nm). The station was operative until December 2010, when the Sun photometer was deployed at another region away from Córdoba. A detailed description of the instruments, data acquisition procedure, and calibration is given by Holben et al. (1998, 2001), and an accurate assessment of the AERONET retrievals can be found in the work of Dubovik et al. (2000). The combined effects of uncertainties in calibration, atmospheric pressure, and ozone amount result in a total uncertainty in the derived AOD values of 0.01–0.02, with the largest errors in the UV region (Eck et al., 1999). Except for the single scattering albedo at 441 nm (SSA_{441}), all the aerosol optical parameters used in this work were level 2.0.

The meteorology in central Argentina is characterized by dry winters with average minimum daily temperature of about 6 °C and rainy summers with an average maximum daily temperature of about 30 °C. The climate is sub-humid with a mean annual precipitation of 790 mm (concentrated mainly in summer time), a mean annual temperature of 17.4 °C and prevailing winds from NE (National Weather Service). The monthly variation of the mean wind speed, average temperature, and total precipitation for the region is shown in Fig. 1, for the 12-year period under study (1999–2010). The soil of the region is loessic and due to the presence of erosive agents it shows weak waves (Kröhling, 1999). During the dry season (April–September) the surrounding hills and mountains are prone to the existence of fires, produced not only accidentally but also intentionally, especially during winter–spring time. In Argentina, available fire databases indicate that, in the average, the burned area covers a wide range of vegetation types, including grasslands (53%), shrub lands (27%) and natural

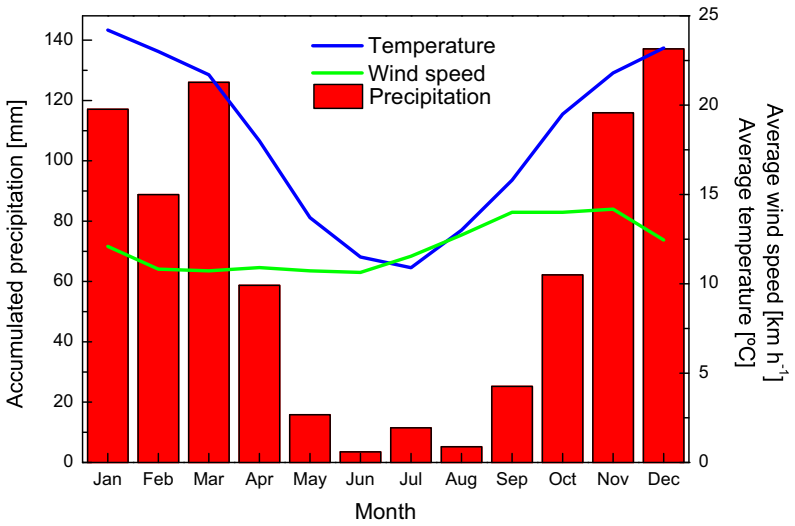

Fig. 1. 12-year averages (1999–2010) of the mean wind speed, average temperature, and total precipitation for Cordoba-CETT station. Data provided by the National Weather Service.

forests (18%). According to regional authorities, fires are caused by negligence or accidents (26%), intentionally for land management (13%) and by natural causes (4%); however, a significant percentage of fires presents unknown causes (57%) (Di Bella et al., 2011).

2.2. Trajectory calculations

All the trajectory calculations presented in this work were carried out by using the HYSPLIT model (Draxler & Hess, 1998, 2004). This model is commonly used for modeling a wide range of conditions related to the regional or long-range transport, dispersion, and deposition of air pollutants. It uses a hybrid approach, in which the calculation employs puff distribution in the horizontal direction and particle dispersion in the vertical (Draxler, 2003). HYSPLIT calculates advection and dispersion using either puff or particle approaches under a Lagrangian framework. The transport and dispersion of a parcel is calculated by assuming the release of a single puff that will expand and split into several puffs when its size exceeds the meteorological grid cell spacing ($2.5^\circ \times 2.5^\circ$ in our calculations). The trajectory calculation is achieved by the time integration of the position of an air parcel as it is transported by the wind field. HYSPLIT can also be used to calculate the source region of an air parcel by moving backward in time, thus indicating its arrival at a receptor at a particular time. In this work, only back trajectories ending at ground level and starting below 5000 m.a.s.l. were considered. The meteorological dataset used in the HYSPLIT simulations is the NCEP/NCAR Reanalysis (Kalnay et al., 1996) with a global domain using a $2.5^\circ \times 2.5^\circ$ grid, 17 pressure levels (up to 10 hPa) and one dataset every 6 h. Although a dataset with a better spatial and temporal resolution is available for the region (GDAS), it provides only data since 2005. Thus, to avoid possible inconsistencies between the two datasets, we decided to use the meteorological data described above for the whole period.

2.3. AERONET optical parameters

The most important aerosol parameter is the AOD, which is calculated as the integral of the atmospheric extinction coefficient from the surface to the top of the atmosphere. As it is measured by direct sun photometry, it requires accurate ground-based solar spectral radiance measurements (Holben et al., 1998). Other aerosol optical properties, such as the size distribution, complex refractive index, fine mode fraction (FMF), and SSA are retrieved based on the AERONET standard inversion methods (Dubovik et al., 2000; Dubovik & King, 2000). Measured aerosol optical depths and almucantar retrievals can be used to derive additional aerosol properties. The wavelength dependence of the AOD is related to the aerosol type and their physical and chemical characteristics. The extinction Ångström exponent (α_{ext}) is calculated from the spectral dependence of AOD using the Ångström equation (Ångström, 1964). For a wavelength range between 440 and 870 nm the calculation is done typically using 440, 500, 675, and 870 nm AOD values and computed by linear regression of ln τ versus ln λ. Values near 0 indicate mainly coarse mode (radius, $r > 1$ μm) aerosol particles, while values near 2 indicate mainly fine or accumulation mode ($r < 1$ μm) aerosol particles (Holben et al., 1998, 2001). The SSA is a variable correlated with the radiative forcing of the Earth's atmosphere. It is defined as the amount of scattering in relation to the total extinction at a small volume of aerosols. The SSA can take values between 0 (a purely absorbing particle) and 1 (a purely scattering particle) and can have important effects on the radiative balance. For example, a change in the SSA from 0.8 to 0.95 can change the sign of the effect on the actinic flux at different altitudes, leading to enhanced actinic fluxes not only above the planetary boundary layer, but also well below its top (Palancar et al., 2013). This has led to major efforts to try to understand, among other things, the amount of soot or "black carbon" in aerosols in a global scale (Hansen et al., 1997). The asymmetry

Table 1
Average aerosol optical properties for period 1999–2010 in Cordoba-CETT station, calculated as the average of daily values. SD is the corresponding standard deviation.

Aerosol optical property	Average	SD
AOD_{340}	0.17	0.07
AOD_{500}	0.10	0.04
$\alpha_{440-870}$	1.2	0.3
$\alpha_{340-440}$	1.2	0.5
SSA_{441}	0.88	0.06
FMF_{500}	0.61	0.11
g_{441}	0.68	0.02

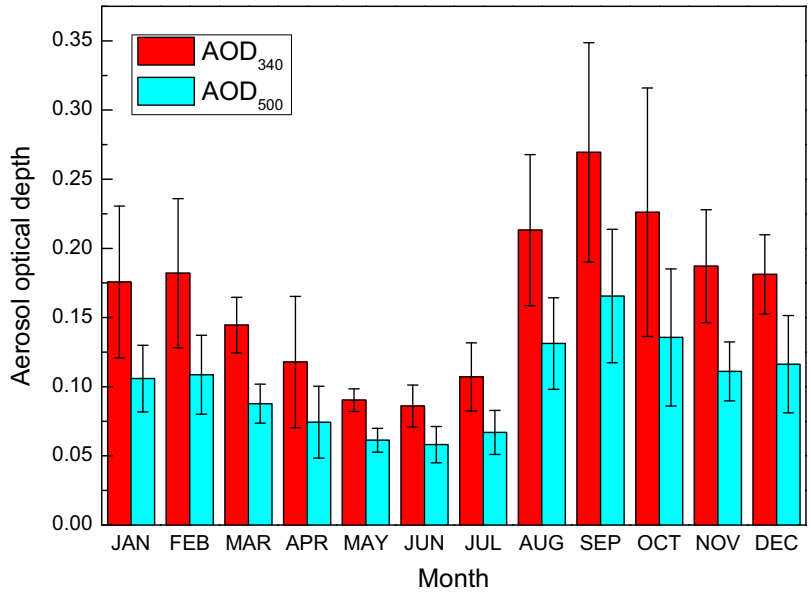

Fig. 2. Monthly variability of AOD_{340} and AOD_{500} from 1999 to 2010 at Cordoba-CETT station.

parameter (g) is a measure of the preferred scattering direction (forward or backward) for the light encountering the aerosol particles. It varies between -1 (for scattering in the backward direction) and 1 (for the forward direction). In this work, the average value of g at 441 nm (g_{441}) is informed but its variation is not analyzed. Finally, the FMF is defined as the ratio of fine mode AOD to total AOD. The FMF derived from the CIMEL sun/sky radiance measurements has been used to represent the dominant aerosol size mode, as FMF provides quantitative information for both fine- and coarse-mode aerosols. Values closer to 1 indicate the dominance of the fine fraction of aerosols. The all-period average values for the aerosol optical properties of interest are shown in Table 1. These values were calculated from the daily average values.

3. Results and discussion

3.1. Monthly variability of aerosol optical properties

In this section, averages values, variation and general behavior of the most important parameters related to aerosols optical properties will be described and analyzed.

The 12-year average monthly variation of AOD at 340 nm (AOD_{340}) and at 500 nm (AOD_{500}), the Ångström parameter at 440–870 nm ($\alpha_{440-870}$), the SSA at 441 nm (SSA_{441}), and the FMF at 500 nm (FMF_{500}) are shown in Figs. 2–5, respectively. For the AODs at both wavelengths is possible to observe the spring seasonal peaks with maximum values around September–October. These months can be considered as a transition period between the dry winter and the rainy summer. That is why this behavior can be explained considering the meteorology of the region during the year. Both, the lack of precipitation and the high wind speed are factors which favor the aerosol loading. From May to August precipitations are very scarce but wind speed is still relatively low (see Fig. 1) leading to the lowest AOD in the year (see Fig. 2). In October and November wind speed is in its maximum but precipitations show a significant increase (reaching a maximum in December) having the effect of moderate the aerosol loading. In September, instead, precipitations are still very sparse and the wind speed is already in its maximum. Thus, low humidity, dryness of the soil, and the strong winds favor the aerosol loading (enriched with soil particles) leading to the highest AOD in the year. Finally, during summer and autumn wind speed and precipitations balance

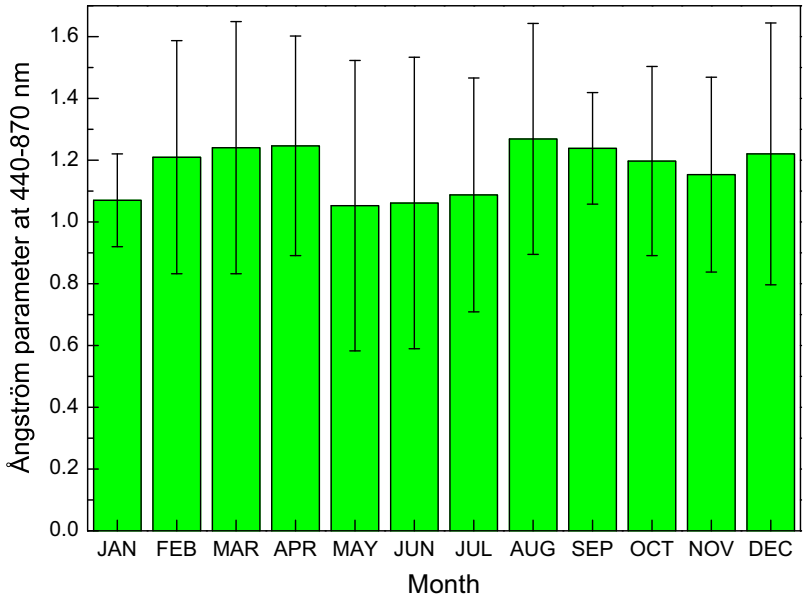

Fig. 3. Monthly variability of $\alpha_{440-870}$ from 1999 to 2010 at Cordoba-CETT station.

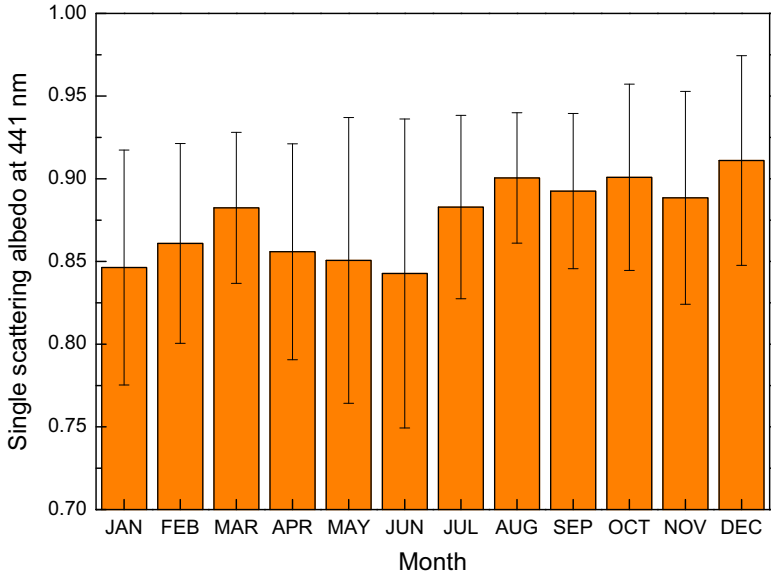

Fig. 4. Monthly variability of SSA_{441} from 1999 to 2010 at Cordoba-CETT station.

the aerosol loading resulting in AOD values around the average. Here, it is important to keep in mind that the shown values are 12-year averages and also that AOD, in absolute terms, are always low.

Results observed in Fig. 3 for $\alpha_{440-870}$ show an annual average value of (1.2 ± 0.3) and only small variations during the year. These values between 1 and 1.5 suggest significant contributions from both accumulation mode and coarse mode aerosols, i.e. mixed aerosols, in all seasons.

Figure 4 shows the average monthly variation of the SSA_{441} (which is the shortest wavelength of AERONET channels). SSA_{441} is used to quantify the aerosol absorption/scattering and, consequently, to distinguish absorbing from non-absorbing aerosols (Lee et al., 2010). In contrast with the other variables, and due to the sparse availability of measurements, SSA values are level 1.5. The lack of SSA data is a consequence of the nature of the data collection method for almucantar retrievals (solar zenith angle (SZA) $\geq 50^{\circ}$) and also to the version 2.0 constraints to assure the data quality ($AOD_{440} > 0.4$) (Dubovik & King, 2000). This parameter shows values going from 0.84 in January to 0.90 in December with an annual average value of 0.88 ± 0.06.

Figure 5 shows the average monthly variation of the FMF_{500}. As seen, all the months have values higher than 0.6, except for May, June and July where the FMF_{500} is around 0.5. By using the particle size and absorption/scattering information, and following the algorithm presented by Lee et al. (2010), we could infer that during those months there is a mixture of fine and

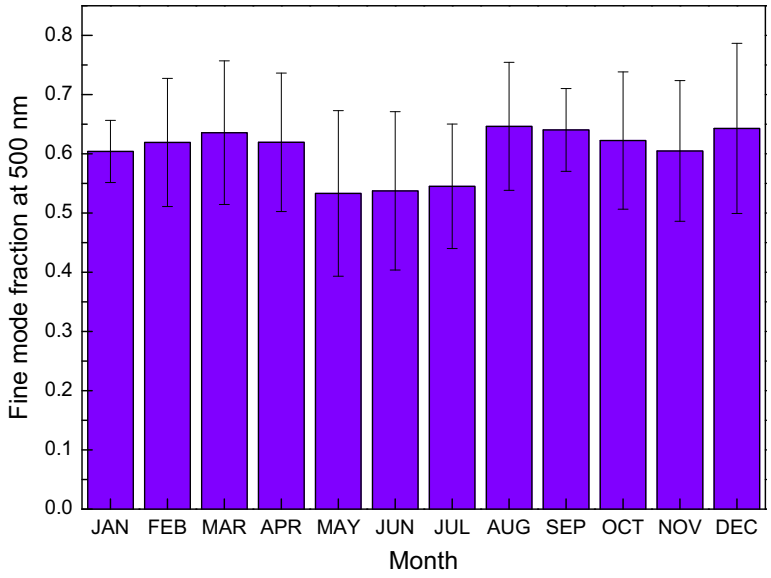

Fig. 5. Monthly variability of FMF_{500} from 1999 to 2010 at Cordoba-CETT station.

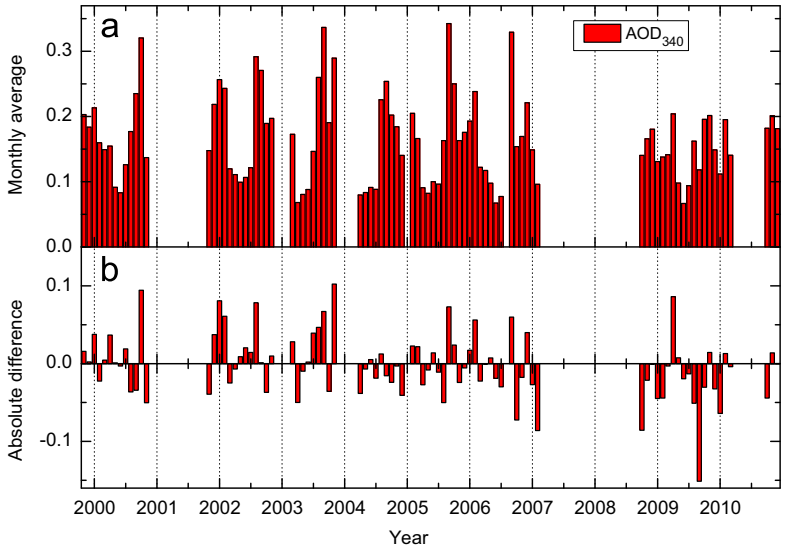

Fig. 6. (a) Inter annual monthly variability of AOD_{340} at Cordoba-CETT station and (b) absolute difference with the average value for the same month, for years 1999–2010.

coarse aerosols. For all the other months and because FMF_{500} is larger than 0.6 and SSA values lay between 0.85 and 0.9, it is possible to say that the dominant aerosol type is composed of carbon particles of moderate absorption.

3.2. *Inter annual variability of aerosol optical properties*

Investigating long-term trends (inter annual) is possible at this station because the records span for several years. In all the years is observed the spring seasonal peak around September–October, when AOD_{340} reaches a maximum value close to 0.35 (Fig. 6a). In order to verify the possible existence of anomalies, in Fig. 6b is represented the monthly inter annual differences, computed as absolute departures (monthly value minus 12-year average value for the same month). The AOD_{340} shows very similar behavior from year to year and the deviations from the mean value are not higher than ± 0.15. From the present data, no trends in the aerosol load are observed. The corresponding plots for AOD_{500} (not shown) follow a similar pattern, with peaks values of about 0.20 in spring. In this case, all inter annual differences were less than ± 0.1.

The monthly variation for the $\alpha_{440-870}$ parameter and the monthly absolute difference are shown in Fig. 7a and b. The corresponding plots for the SSA_{441} and the FMF_{500} are shown in Figs. 8 and 9, respectively. Here clearly emerges an important difference for the year 2004 where $\alpha_{440-870}$ increases 1 unit above the average value to reach values larger than 2, the FMF_{500} increases up to 0.25 units to reach values close to 0.9, and the SSA increased around 0.13 units to reach values close to 1. These results show important changes in the optical properties of the aerosols. To investigate the possible causes

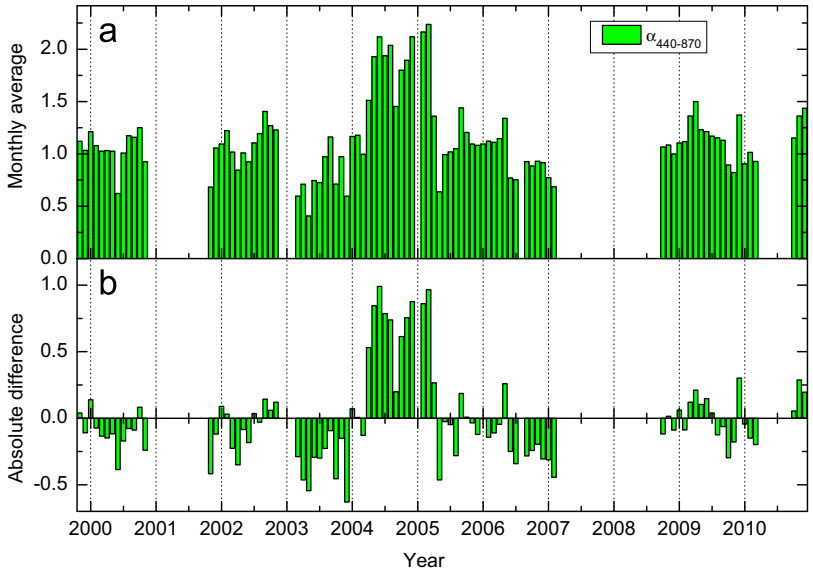

Fig. 7. (a) Inter annual monthly variability of $\alpha_{440-870}$ at Cordoba-CETT station and (b) absolute difference with the average value for the same month, for years 1999–2010.

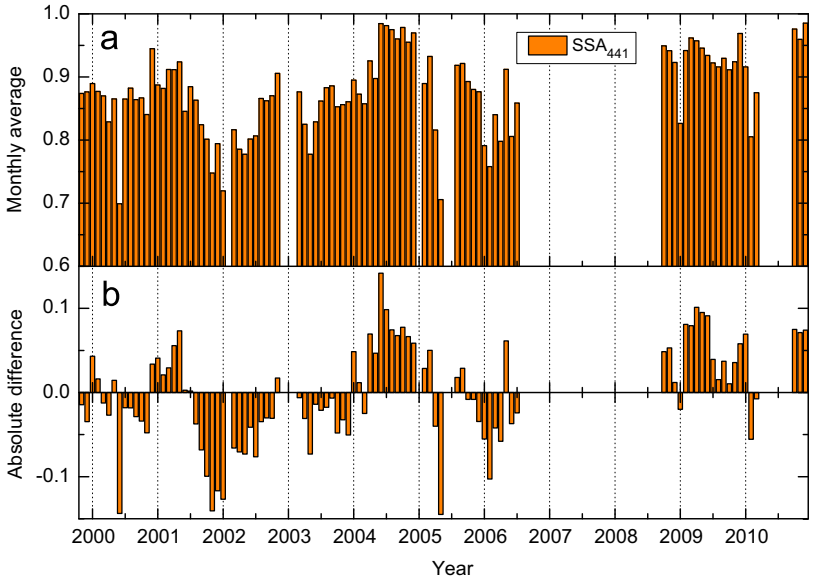

Fig. 8. (a) Inter annual monthly variability of SSA_{441} at Cordoba-CETT station and (b) absolute difference with the average value for the same month, for years 1999–2010.

of these differences, we compared the annual average values of the optical properties for 2004 respect to the average value of the 12-year period. Here, we found that $\alpha_{440-870}$ increased from (1.2 ± 0.3) to (1.7 ± 0.4), the SSA_{441} increased from (0.88 ± 0.06) to (0.94 ± 0.05), and the FMF_{500} also increased from (0.61 ± 0.1) to (0.74 ± 0.1). However, AOD_{340} value for this year (0.15 ± 0.07) is not significantly different from the average value of the whole period (0.17 ± 0.07). From this analysis we can conclude that during this period there was not an important change in the total aerosol load but a change in the size and type of aerosol affecting the region, as the aerosols changed from absorbing accumulation mode to scattering fine mode. This result cannot be cataloged as an isolated episode because it lasted for around a year, as seen in Fig. 7. An explanation for this anomalous behavior was investigated carrying out a back trajectory analysis by using the HYSPLIT model (see Section 3.3).

3.3. Air mass correlation with optical properties

Different aspects of the atmospheric dynamics in the region were investigated using the HYSPLIT model. This model was used to analyze and correlate the origin of the air masses with the optical properties of the aerosols by moving backward in time to calculate the position of an air parcel up to 96 h before arriving to the Cordoba-CETT station.

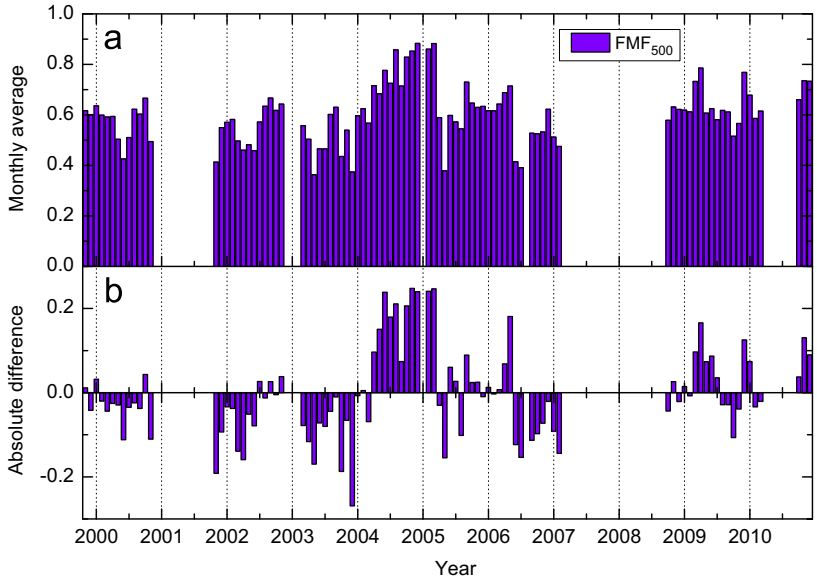

Fig. 9. (a) Inter annual monthly variability of FMF_{500} at Cordoba-CETT station and (b) absolute difference with the average value for the same month, for years 1999–2010.

Figure 10a–c shows the grid with the position of all the air masses 24, 48, and 72 h before arriving to the Cordoba-CETT site, being the intensity of the color proportional to the number of trajectories that have that position. Figure 10 was obtained by calculating one back trajectory for each hour of each day of each year in the period 1999–2010 to know the path and position of the air parcel up to 96 h before arriving to the measurement site. Then, the trajectories were clustered in a square cell grid depending on its position 24, 48 and 72 h before arriving to the site. Each cell is 50 km wide and the grid covers an area of 2200 × 2200 km centered on the measurement site. From Fig. 10c it is observed that 72 h before arriving to the site, the air masses are mostly located on the East and, in a minor extension, on the Northwest region of Argentina and North of Chile. However, 24 h before the air masses are concentrated in the Northeast region of Córdoba. This is entirely consistent with previous studies in Córdoba, where it was shown that the predominant direction of the winds is the Northeast (Olcese & Toselli, 2002). Although the figure shows the accumulated behavior during the 12-year period, a similar pattern has been observed for each year, which is also consistent with the recurring meteorology of Córdoba region. Although within each year the distribution of the air masses 24 h before shows small to moderate variations, the Northeast direction is still the most important for most months.

Here, it should be kept in mind that any trajectory given by this model is representative of the large scale circulation, and as such, may be used to suggest a potential source region. However, trajectory models are subject to uncertainties arising from interpolations of sparse meteorological data, assumptions regarding to vertical transport, observational errors, sub-grid-scale phenomenon, turbulence, convection, evaporation and condensation (Polissar et al., 1999). Thus, it does not imply that a particular air parcel sampled at the trajectory destination had exactly followed this path. Trajectories were grouped depending on its starting position in a grid, which is spaced every 800 km in both latitude and longitude (See Figs. 11 and 12).

To analyze if the anomalous observed values of the different aerosol optical parameters during 2004 were a consequence of a change in the air mass trajectories pattern, we compared back trajectory simulations for this year against all the years of the period. To correlate the trajectory of the air mass with the value of a given aerosol optical property, a 96 h back trajectory was started for each hour with a recorded value of the aerosol optical property of interest. Then, trajectories were clustered, as previously described, and a histogram of the values of the chosen aerosol optical parameter was created for the trajectories starting in each cell. Trajectories that start outside the boundary limits where discarded (less than 0.4% of the total trajectories). As $\alpha_{440-870}$ is the variable that shows the larger difference between 2004 and the 12-year period, it will be used here for the analysis. The resulting histograms for the entire period and for the year 2004 are shown in Figs. 11 and 12, respectively. The percentage shown in each cell is relative to the total number of trajectories, giving, in this way, an idea of the number of trajectories starting in the corresponding cell. Thus, regarding to the position of the air masses, the histograms show no large differences between the period 1999–2010 and the year 2004 for back trajectories starting 96 h before arriving to the monitoring site. Equivalent plots for 24, 48, and 72 h have been analyzed and similar behaviors, respect to frequency and location of the air masses, were observed.

Concerning the increase in the $\alpha_{440-870}$ values for 2004, they were observed in all the cells, but in different magnitudes. In fact, the average value of $\alpha_{440-870}$ for air masses coming from the West region (defined as the ten cells on the left of the site) increased from 1.08 to 1.69 (57% increase), in contrast with the 1.28 to 1.51 (18% increase) for air masses coming from the East (ten cells on the right of the site). Air masses coming directly from the North or the South (two cells above/below the site, respectively) also show an important increase (42 and 46% respectively). The corresponding plots for AOD_{340} (not shown)

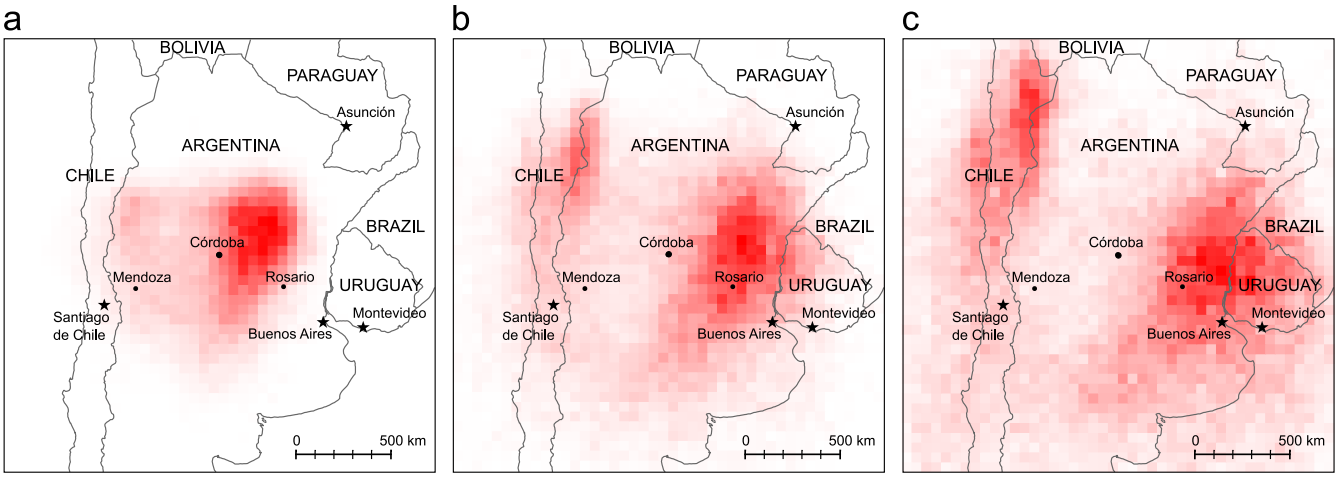

Fig. 10. 2-D histogram for 24, 48 and 72 h back trajectories for every hour during the period 1999–2010, calculated by the HYSPLIT model. Darker cells mark higher count of trajectories. Maximum values for each figure are (a) 868 (24 h), (b) 410 (48 h), and (c) 231 (72 h).

show a similar pattern when 2004 is compared against the whole period. Although 96 h before a considerable number of air masses are located over the sea, the contribution of marine aerosols was neglected because the observed properties do not correspond with the known optical and physical properties of this kind of aerosols. The differences cannot be either allocated to changes in the wind patterns or other meteorological conditions, as no relevant differences were observed. Considering the precedent results, the explanation for this period with anomalous optical properties relies on long-range transport, although the specific causes or sources are not entirely clear yet. Thus, the possible responsible for the observed differences is a temporary source, located in the West of the site, emitting a large fraction of small aerosols with scattering properties larger than those usually measured in the Cordoba-CETT station.

3.4. *Episodes with higher AOD value than the average*

Short-term changes in the aerosol optical properties are very specific to the region of the station and can often be explained by tracing back the air mass history during these events. These episodes usually lead to high AOD values on specific days throughout the year. That is why the study of the severe aerosol episodes has a significant importance from the climatic, atmospheric and human health points of view. Days with severe aerosol and pollution conditions may be related to enhanced anthropogenic emissions, intense dust outflows, increased biomass and agriculture burning, absence of precipitation, longer aerosol lifetime, temperature inversions, and lower mixing height (Kaskaoutis et al., 2013). To detect the presence of higher-than-average values of a given optical property we looked at the day-to-day differences. Figure 13a shows the daily AOD_{500} variation for the period while Fig.13b shows the differences between the daily average values against the average for all the corresponding days of the 12-year period. From this figure, we could observe several cases where the daily AOD_{500} values are much higher than the average. From all these cases, we have selected for the analysis 3 of them, as they cover different causes for the AOD_{340} and AOD_{500} increments. All the values presented in these analyses are daily averages. These high-load aerosol episodes are presented in Table 2. In the trajectory analysis used in this section to explain single-day episodes, an ensemble of trajectories (27 trajectories for each hour, shifting the meteorology grid plus/minus 1 grid point in latitude and longitude and 0.01 sigma units in the vertical), has been used in order to minimize inconsistencies in the meteorological fields (Draxler, 2003). The data for the analysis of the fire locations was obtained from the Moderate Resolution Imaging Spectroradiometer (MODIS) sensor on board Terra and Aqua platforms (product MOD 14, Thermal Anomalies – Fires and Biomass Burning) for the period of interest (Justice et al., 2002).

In one of the episodes, on 21 December 2006, an AOD_{340} value of 0.76 and an AOD_{500} value of 0.77 were measured. These values are much larger than the average and unexpected for this time of the year. Among the possible explanations for these anomalous AODs, we disregarded the possibility of important fires in the surrounding regions. Although some minor fires can be seen in the MODIS fire counts maps, the back trajectories calculated by using the HYSPLIT model show that the air masses are not coming from the regions where fires were detected but from the West direction. Furthermore, the $\alpha_{440-870}$ value for that day was 0.994, which indicates the dominance of large particles, in contraposition of what it could be expected because of a fire. Unfortunately, AERONET does not report the value of SSA for that day, which could shed light on this analysis. A possible explanation for this episode involves the same factors responsible for the increments in the AODs every year in the winter–spring period, i.e. the Córdoba meteorology, described in Section 2.1.

On 9 September 2005, AOD_{340} reached a value of 1.073 and AOD_{500} a value of 0.607. The $\alpha_{440-870}$ exponent of 1.780 indicates the presence of mostly fine particles, which is also corroborated through the value of the FMF_{500} of 0.912. These results, together with a value for the SSA_{441} of 0.919, point to fires as the likely responsible for the high AODs values. Looking at the path of the air mass arriving to the site we observe that the air masses are coming from the northeast region of Argentina and Paraguay, where the MODIS sensor detected numerous fires. Fire density in those regions begins to increase

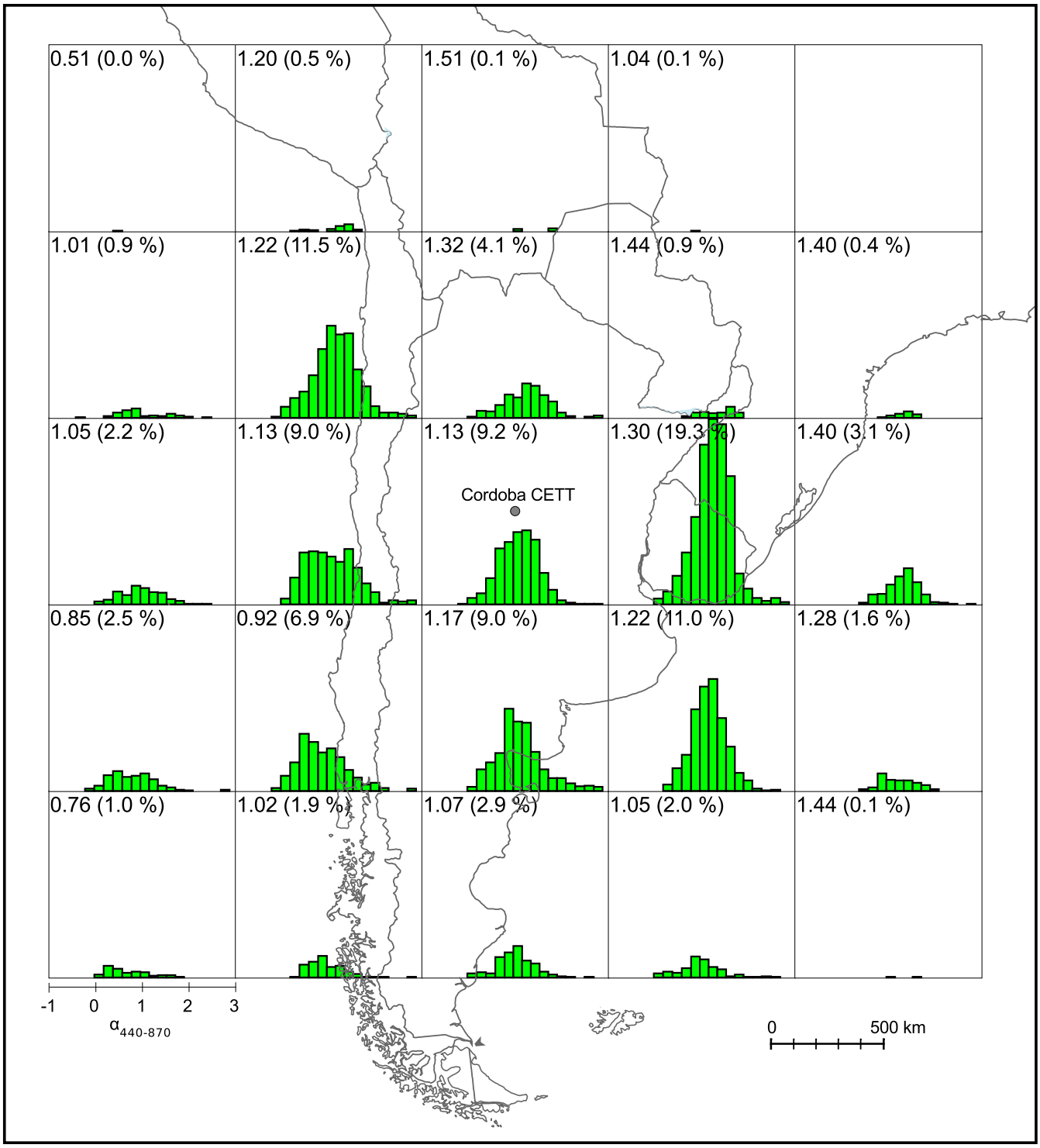

Fig. 11. Histograms relating HYSPLIT-calculated air parcel position 96 h before arriving to Cordoba-CETT station and $\alpha_{440-870}$ for years 1999–2010. Numbers shown in each cell represent the average value and the percentage of the total cases. The $\alpha_{440-870}$ scale shown is the same for all the cells.

in June–July due to the onset of several meteorological conditions, such as strong winds with a NNE direction and low relative humidity, among others. The end of this fire season varies according to the beginning of the rainy season (October–November) (Di Bella et al., 2011).

The episode of 27 August 2002 can be explained combining the two previously described situations. On this day, the trajectories arrived to Cordoba-CETT from the Northeast region, where several biomass burning spots were detected by the MODIS instrument. The AOD_{340} and AOD_{500} values during this episode were 1.399 and 0.861, respectively. These values represent the highest average daily values recorded at the station for the corresponding wavelengths. An $\alpha_{440-870}$ value of 1.657, together with an SSA_{441}value of 0.892 and a FMF_{500} value of 0.912 lead to the picture of a large amount of fine

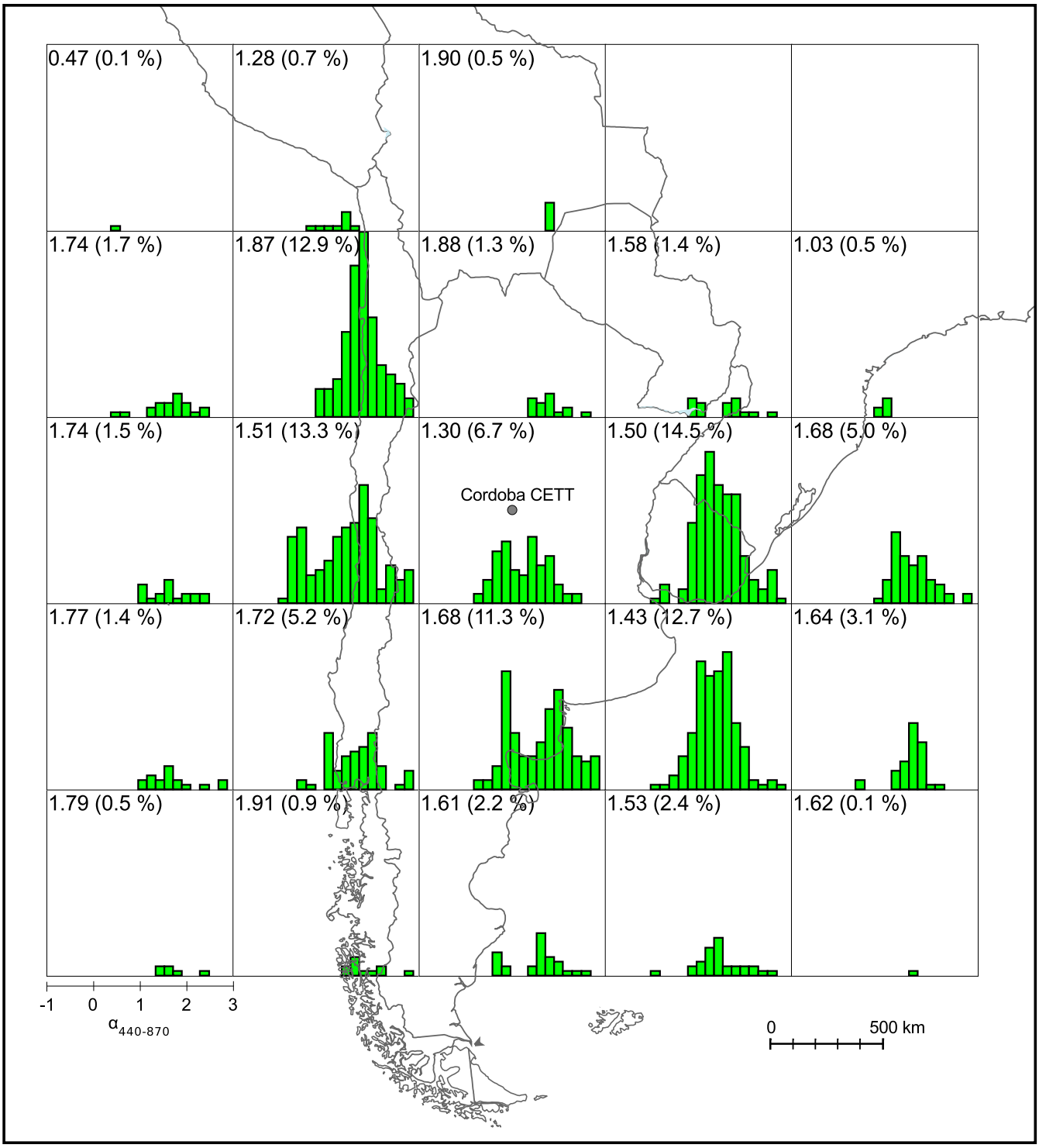

Fig. 12. Histograms relating the HYSPLIT-calculated air parcel position 96 h before arriving to Cordoba-CETT station and $\alpha_{440-870}$ for year 2004. Numbers shown in each cell represent the average value and the percentage of the total cases. The $\alpha_{440-870}$ scale shown is the same for all the cells.

particles, having probably an origin related to biomass burning, although its source was not fully corroborated by the MODIS instrument.

4. Summary and concluding remarks

The ground-based long-term database provided by AERONET Cordoba-CETT station allowed a comprehensive analysis of the aerosol optical properties to establish the climatology of the aerosols in the central region of Argentina in the period of 1999–2010. The climatology of aerosols in the Córdoba region is defined by a low burden of particles ($AOD_{340} = 0.17 \pm 0.07$;

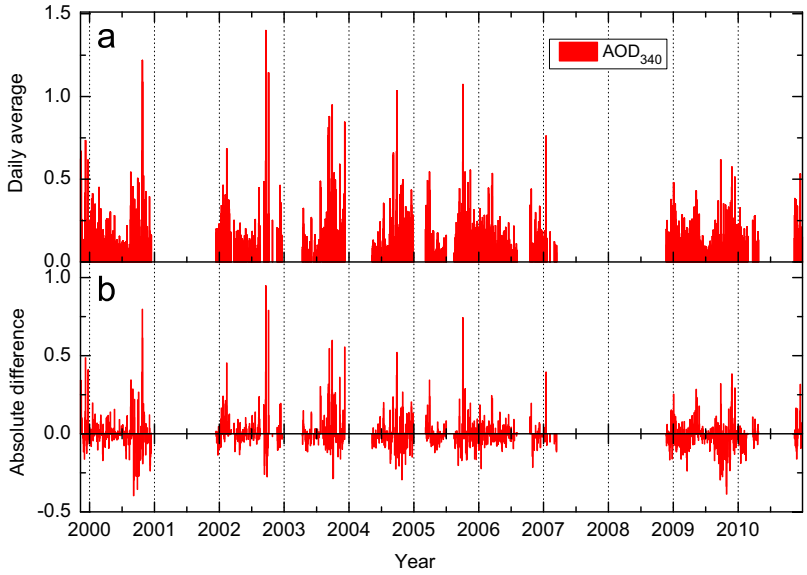

Fig. 13. (a) Inter annual daily variability of AOD_{500} at Cordoba-CETT station and (b) absolute difference with the average value for the same day, for years 1999–2010.

Table 2
Daily average of the aerosol optical properties for high AOD episodes recorded at Cordoba-CETT station.

Day	AOD_{500}	AOD_{340}	$\alpha_{440-870}$	SSA_{441}	FMF_{500}
21 December 2006	0.770	0.761	0.994	N/A	0.999
9 September 2005	0.607	1.073	1.780	0.919	0.912
27 August 2002	0.861	1.399	1.657	0.892	0.912

$AOD_{500} = 0.10 \pm 0.04$), characterized by a mixture of the coarse and fine modes ($\alpha_{440-870} = 1.2 \pm 0.3$) and with moderate absorption properties ($SSA_{441} = 0.88 \pm 0.06$). FMF_{500} and g_{441} are 0.6 ± 0.1 and 0.68 ± 0.02, respectively. The AOD variation along the year is determined by the meteorology, with recurring maxima in the winter–spring period (because sparse precipitations and high wind speed). The monthly variation shows low average values, ranging from 0.17 in February down to 0.12 in April, very low values from May to June (less than 0.10) and a sustained increase from July to September, reaching a value of 0.26. All the other optical properties show smoothed monthly variations. From the present aerosol data, no long-term trends were observed in any of the analyzed optical properties. AOD values larger than 0.4 were only registered during specific episodes, typically lasting no more than two days. These isolated episodes were detected, analyzed, and explained by the combined used of back trajectories, meteorology datasets, and the observed aerosol optical properties. Most of these episodes have their origin in fires and/or in long-range transport. Only one long-lasting anomaly was identified during the year 2004. The analysis shows that the possible responsible for the observed differences is an unknown temporary source, located in the West of the site, which emitted a moderate amount of aerosols with a large fraction of small particles and scattering properties larger than those usually measured in the Cordoba-CETT station (probably sulfates). The low AOD values and the latitude of the measuring site seriously limit the availability of level 2 SSA_{441} data for this region. This is a consequence of the application of the version 2.0 constraints to assure the data quality ($AOD_{440\ nm} > 0.4$) and also because of the nature of the data collection method for almucantar retrievals ($SZA \geq 50^{\circ}$).

Air masses arrive to Córdoba region from the Northeast direction although specific remote sources which could contribute to the observed properties have not been studied yet. One of the main drawbacks for carrying out trajectory analysis in our region is the lack of highly resolved meteorological fields in both space and time. An improvement in the availability of these resources would lead to a better resolution of the atmospheric physics and to the ability of better infer the movement, mixing and transport of atmospheric constituents.

As the AERONET Cordoba-CETT station is not longer in operation, this work compiles the whole set of available data and, thus, can be used as a reference in future works where aerosol optical properties are needed. Hence, the presented results will help to improve our understanding of the direct and indirect radiative forcing by aerosols in the region.

Acknowledgments

We thank CONICET, FONCYT (Préstamo BID PICT 309) and SeCyT (UNC) for partial support of the work reported here. We especially thank the PI and his staff for establishing and maintaining the Córdoba-CETT site used in this investigation.

We also thank Brent Holben for permission to use the AERONET data and CONAE (Comisión Nacional de Actividades Espaciales) staff for looking after the instrument deployed in this site.

References

Achad, M., López, M.L., Palancar, G.G., & Toselli, B.M. (2013). Retrieving the relative contribution of aerosol types from single particle analysis and radiation measurements and calculations: a comparison of two independent approaches. *Journal of Aerosol Science*, *64*, 11–23.

Andrada, G.C., Palancar, G.G., & Toselli, B.M. (2008). *Using the optical properties of aerosols from the AERONET database to calculate surface solar UV-B irradiance in Córdoba, Argentina: comparison with measurements*. *Atmospheric Environment*, 426011–6019.

Ångström, A. (1964). The parameters of atmospheric turbidity. *Tellus*, *16*(1), 64–75.

Di Bella, C.M., Fischer, M.A., & Jobbágy, E.G. (2011). Fire patterns in north-eastern Argentina: influences of climate and land use/cover. *International Journal of Remote Sensing*, *32*(17), 4961–4971.

Draxler, R.R. (2003). Evaluation of an ensemble dispersion calculation. *Journal of Applied Meteorology*, *42*(2), 308–317.

Draxler, R.R., & Hess, G.D. (1998). An overview of the HYSPLIT_4 modelling system for trajectories, dispersion and deposition. *Australian Meteorological Magazine*, *47*, 295–308.

Draxler, R.R., & Hess, G.D. (2004). Description of the Hysplit_4 modeling system. NOAA Technical Memorandum ERL ARL-24.

Dubovik, O., & King, M.D. (2000). A flexible inversion algorithm for retrieval of aerosol optical properties from Sun and sky radiance measurements. *Journal of Geophysical Research: Atmospheres*, *105*(D16), 20673–20696.

Dubovik, O., Smirnov, A., Holben, B.N., King, M.D., Kaufman, Y.J., Eck, T.F., & Slutsker, I. (2000). Accuracy assessments of aerosol optical properties retrieved from Aerosol Robotic Network (AERONET) Sun and sky radiance measurements. *Journal of Geophysical Research: Atmospheres*, *105*(D8), 9791–9806.

Eck, T.F., Holben, B.N., Reid, J.S., Dubovik, O., Smirnov, A., O'Neill, N.T., & … Kinne, S. (1999). Wavelength dependence of the optical depth of biomass burning, urban, and desert dust aerosols. *Journal of Geophysical Research: Atmospheres*, *104*(D24), 31333–31349.

Fleming, Z.L., Monks, P.S., & Manning, A.J. (2012). Review: untangling the influence of air-mass history in interpreting observed atmospheric composition. *Atmospheric Research*, *104–105*, 1–39.

Flynn, J., Lefer, B., Rappenglu, B., Leuchner, M., & Crawford, J. (2010). Impact of clouds and aerosols on ozone production in Southeast Texas. *Atmospheric Environment*, *44*, 4126–4133.

Hansen, J., Sato, M., & Ruedy, R. (1997). Radiative forcing and climate response. *Journal of Geophysical Research: Atmospheres*, *102*(D6), 6831–6864.

Holben, B.N., Eck, T.F., Slutsker, I., Tanré, D., Buis, J.P., Setzer, A., & … Smirnov, A. (1998). AERONET—a federated instrument network and data archive for aerosol characterization. *Remote Sensing of Environment*, *66*(1), 1–16.

Holben, B.N., Tanré, D., Smirnov, A., Eck, T.F., Slutsker, I., Abuhassan, N., & Zibordi, G. (2001). An emerging ground-based aerosol climatology: aerosol optical depth from AERONET. *Journal of Geophysical Research: Atmospheres*, *106*(D11), 12067–12097.

Justice, C., Giglio, L., Korontzi, S., Owens, J., Morisette, J., Roy, D., & Kaufman, Y. (2002). The MODIS fire products. *Remote Sensing of Environment*, *83*(1–2), 244–262.

Kalnay, E., Kanamitsu, M., Kistler, R., Collins, W., Deaven, D., Gandin, L., & Joseph, D. (1996). The NCEP/NCAR 40-year reanalysis project. *Bulletin of the American Meteorological Society*, *77*(3), 437–471.

Kaskaoutis, D.G., Sinha, P.R., Vinoj, V., Kosmopoulos, P.G., Tripathi, S.N., Misra, A., & Singh, R.P. (2013). Aerosol properties and radiative forcing over Kanpur during severe aerosol loading conditions. *Atmospheric Environment*, *79*, 7–19.

Kröhling, D.M. (1999). Sedimentological maps of the typical loessic units in North Pampa, Argentina. *Quaternary International*, *62*(1), 49–55.

Lee, J., Kim, J., Song, C.H., Kim, S.B., Chun, Y., Sohn, B.J., & Holben, B.N. (2010). Characteristics of aerosol types from AERONET sunphotometer measurements. *Atmospheric Environment*, *44*(26), 3110–3117.

Madronich, S. (1987). Photodissociation in the atmosphere: 1. Actinic flux and the effects of ground reflections and clouds. *Journal of Geophysical Research: Atmospheres*, *92*(D8), 9740–9752.

Olcese, L.E., & Toselli, B.M. (2002). Some aspects of air pollution in Córdoba, Argentina. *Atmospheric Environment*, *36*(2), 299–306.

Palancar, G.G., Lefer, B.L., Hall, S.R., Shaw, W.J., Corr, C.A., Herndon, S.C., & Madronich, S. (2013). Effect of aerosols and NO2 concentration on ultraviolet actinic flux near Mexico City during MILAGRO: measurements and model calculations. *Atmospheric Chemistry and Physics*, *13*(2), 1011–1022.

Polissar, A.V., Hopke, P.K., Paatero, P., Kaufmann, Y.J., Hall, D.K., Bodhaine, B.A., & Harris, J.M. (1999). The aerosol at Barrow, Alaska: long-term trends and source locations. *Atmospheric Environment*, *33*(16), 2441–2458.

Solomon, S., Qin, D., Manning, M., Chen, Z., Marquis, M., Avery, K.B., Tignor, M., & Miller, H.L. (2007). *Climate Change 2007: the Physical Science Basis – Contribution of Working Group I to the Fourth Assessment Report of the Intergovernmental Panel on Climate Change*. Cambridge University Press, Cambridge: UK/New York.

Srivastava, A.K., Tripathi, S.N., Dey, S., Kanawade, V.P., & Tiwari, S. (2012). Inferring aerosol types over the Indo-Gangetic Basin from ground based sunphotometer measurements. *Atmospheric Research*, *109–110*, 64–75.

Viana, M., Kuhlbusch, T.A.J., Querol, X., Alastuey, A., Harrison, R.M., Hopke, P.K., & … Hitzenberger, R. (2008). Source apportionment of particulate matter in Europe: A review of methods and results. *Journal of Aerosol Science*, *39*(10), 827–849.

Zawadzka, O., Markowicz, K.M., Pietruczuk, A., Zielinski, T., & Jaroslawski, J. (2013). Impact of urban pollution emitted in Warsaw on aerosol properties. *Atmospheric Environment*, *69*, 15–28.